Received: 17 October 2019 | Revised: 10 January 2020 | Accepted: 30 January 2020
DOI: 10.1002/qua.26181

FULL PAPER

International Journal of QUANTUM CHEMISTRY WILEY

The solvent effect on a styryl-bodipy derivative functioning as an AND molecular logic gate

Demeter Tzeli[1,2] | Ioannis D. Petsalakis[1] | Giannoula Theodorakopoulos[1]

[1]Theoretical and Physical Chemistry Institute, National Hellenic Research Foundation, Athens, Greece

[2]Laboratory of Physical Chemistry, Department of Chemistry, National and Kapodistrian University of Athens, Athens, Greece

Correspondence
Demeter Tzeli and Ioannis D. Petsalakis, Theoretical and Physical Chemistry Institute, National Hellenic Research Foundation, 48 Vassileos Constantinou Ave., Athens 116 35, Greece.
Email: dtzeli@eie.gr; tzeli@chem.uoa.gr (D. T.) and Email: idpet@eie.gr (I. D. P.)

Funding information
European Regional Development Fund; NSRF 2014-2020

Abstract

We study via DFT and TDDFT calculations the photophysical processes of a styryl-bodipy derivative, (**1**), of its monometallic complexes **1-M**$^{2+}$ (M = Ca, Zn, and Hg), and its trimetallic complex (**2**) unprotonated, protonated and complexed with water molecules in water solvent and in acidic conditions. The main targets of this study are to gain information regarding published reports on fluorophore species mentioning that fluorescent switching results from trace water, to study how **1** behaves in water solvent which is a common used solvent for molecular logic gates (MLG), and how it behaves in acidic conditions. We conclude that in water solvent, as in acetonitrile solvent (which was found before both theoretically and experimentally) there will be a quenching of emission spectra in **1** and **1-M**$^{2+}$ and a retaining of emission in **2**. However, contrary to acetonitrile solvent, in water, a weak peak will be observed for **1** and **1-M**$^{2+}$, due to a small ratio of reversible protonation, showing that in acetonitrile **1** acts as a better MLG candidate than in water solvent. On the other hand, in acidic conditions all five species will emit and as a result, **1** will not be an AND MLG, showing that the selection of the solvent conditions is crucial for a species to act as an MLG candidate. Finally, we conclude that the retaining of emission is accomplished by the simultaneous tetrahedral geometry of all three aniline N atoms.

KEYWORDS
charge-transfer, DFT calculations, molecular logic gate, spectra, styryl-bodipy

1 | INTRODUCTION

Fluorescence chemosensors and molecular switches present applications in diverse sciences, such as chemistry, electronics, materials, and medicine.[1–4] Molecules respond to changes in their environment, such as changes of pH, temperature, solvent, viscosity, the presence of various ions, of neutral species, and so on.[1–12] As a result, in response to these modulations, molecules can exhibit differences in their ground or excited electronic states, with accompanying modifications in the absorption and/or emission intensity and wavelength. Such changes can be related to the operation of fluorescence chemosensors, molecular switches, and logic gates (via the familiar Boolean logic where the modulators correspond to the inputs and the observed changes correspond to the outputs).[5–21] As a consequence, the field of molecular logic gates and generally of chemosensors and molecular switches is very active and many research groups around the world work on these subjects.[5–45]

The majority of fluorescence chemosensors and molecular switches are based on the "on-off" or "off-on" response of photoinduced electron transfer (PET),[36–38] because PET produces very sharp changes in the signal intensity and it can be modulated in such a way as to generate significant changes in the emission wavelengths. The impact of PET on UV-vis absorption is often negligible and other effects, such as intramolecular charge transfer (ICT) could affect the UV-vis absorption.[43,44] Finally, it should be noted that there are also fluorescent switches which are not built based on PET, but on other mechanisms, such as twisted intramolecular charge transfer.[45]

 © 2020 Wiley Periodicals, Inc.

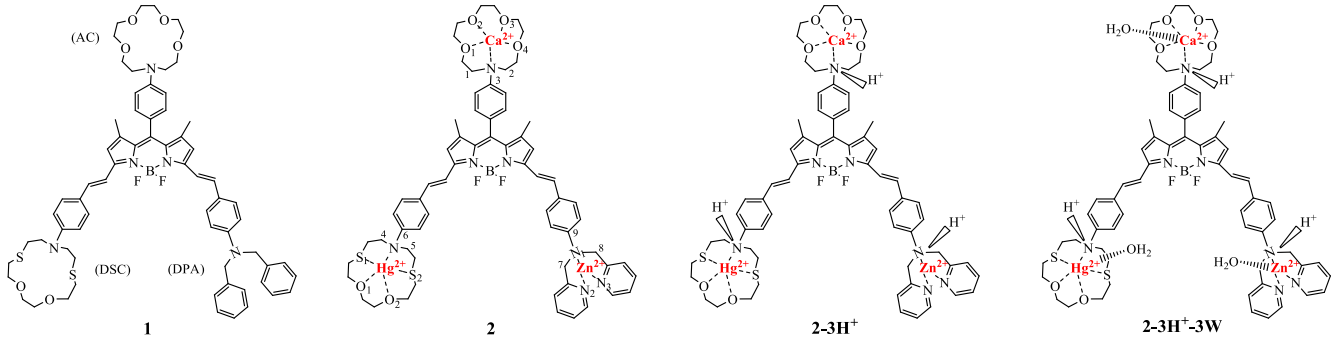

SCHEME 1 Calculated structures of the **1**, **2**, **2-3H$^+$**, and **2-3H$^+$-3W** molecules

Recently, the photophysical processes of a styryl-bodipy derivative (**1**), which acts as a three metal-cation-receptor fluorophore and as a three input AND molecular logic gate were studied theoretically by our group[35] in view of earlier experimental work by Bozdemir et al[12] **1** consists of a central group of boron-dipyrromethene (BODIPY), that is, dipyrromethene complexed with a disubstituted boron atom, a BF_2 unit, which acts as a fluorescent dye and three groups which are bonded to BODIPY, that is, an azacrown ether (AC), a dithia-azacrown ether (DSC), and a dipicolylamine (DPA) units, see Scheme 1. The metals are selectively attached to the ligands, that is, Ca^{2+} is complexed to the AC ligand, Hg^{2+} to the DSC ligand, and Zn^{2+} to the DPA ligand, resulting in the trimetallic complex **2**, see Scheme 1. Reproducing the experimental conditions, the **1**, **2** species and the monometallic complexes **1-M^{2+}**, where M = Ca, Zn, and Hg were calculated in acetonitrile. Our data regarding the absorption and emission spectra were in excellent agreement with experimental ones. It was found that the observed quenching of emission of **1** and of the monometallic complexes may be attributed to the fact that their first excited state is a charge-transfer (CT) state whereas this does not happen for the complex **2**. In this previous work, apart from the rationalization of the available experimental data we obtained information on the appropriate computational approach for successful prediction of molecular logic gate candidates, that is, we found that the inclusion of corrections to the excitation energies for nonequilibrium solvent effects, as also, for the case of **1-Ca^{2+}**, the additional explicit inclusion of the solvent were necessary for the correct ordering of the excited states. Additionally, we explained why the given combination of three different receptors with the BODIPY fluorophore results in the observed interesting optoelectronic responses of **1**, that is, it is a 3-input AND MLG.

In the present work, we are going to expand our work on the styryl-bodipy derivative in order to provide experimentalists with further information regarding this MLG candidate because: (a) In the literature, there are reports of fluorescent switching resulting from the presence of trace water, which can coordinate with metal ions and the azacrown ether becomes protonated rather than complexing with the metal ion.[18–20] The fact that **1** has three receptors that are all protonable brings up this concern. (b) Moreover, water is a common solvent used in MLG candidates,[22] and a reasonable question was raised, "how would **1** behave in water solvent?" (c) Finally, it could be informative to learn about the photophysics of **1** under acidic conditions, that is, where all three of the aniline nitrogen atoms are protonated and water is complexed to metals.

Thus, in the present paper, we study theoretically the photophysical processes of unprotonated and protonated at the aniline nitrogen atoms **1**, its monometallic complexes **1-M^{2+}**, and its trimetallic complex **2**, in water solvent. Additionally, all above species were complexed or attached with one or three water molecules in order to consider explicit addition of the solvent. The relevant questions are: Does **1** still act as an AND MLG? What are the differences on the absorption and emission spectra of **1**, **1-M^{2+}**, and **2** in acetonitrile, water solvent and in acid conditions? Are the spectra similar? Which is the key factor for the retaining of the emission in all calculated species regardless of the conditions? It should be noted that our previous studies[21,35] have provided us with all necessary know-how of computational approach for successful prediction of molecular logic gate candidates and molecular switches, which will be used in the present study.

2 | METHODOLOGY

The DFT and TDDFT calculations were carried out using the PBE0[46] functional in conjunction with the 6–31G(d,p)[47] for H, C, O, N, S, Ca, Zn, and LANL2TZ[48] basis sets for Hg in water solvent. This methodology predicted the best results for **1**, **1-M^{2+}**, and **2** in acetonitrile solvent compared to the available experimental data and for this reason it is applied for the present calculations. Moreover, its applicability has been tested previously on calculations of the absorption and emission spectra in similar systems, including complexes of crown ethers.[21,49]

At first, conformational analyses have been carried out. All species were fully geometry optimized in the ground state (S_0), in the first (S_1), and in the second excited singlet state (S_2) in water (ε = 78.3553) solvent employing the polarizable continuum model (PCM).[50] In our previous study,[35] acetonitrile was used as a solvent in order to reproduce the experimental conditions,[12] while here the water solvent was used since we wanted to examine the photophysical properties of **1**, **1-M^{2+}**, and **2** in water solvent and in acidic conditions.

Here, we study via density functional theory (DFT) and time dependent DFT (TDDFT), in water solvent, the electronic structure of **1**, its monometallic complexes of **1**, **1-M^{2+}**, with M = Ca^{2+}, Zn^{2+}, and Hg^{2+}, that is, **1-Ca^{2+}**, **1-Zn^{2+}**, and **1-Hg^{2+}**, the trimetallic complex of **1** with all three M^{2+} cations, that is, **2**, the protonated complexes with three H^+, that is, **1-3H$^+$**, **1-M^{2+}-3H$^+$** and **2-3H$^+$**, and the above species complexed with one or three water molecules, that is, **1-3W**, **1-M^{2+}-3W**, **1-M^{2+}-3H$^+$-1W**, **1-M^{2+}-3H$^+$-3W**, and **2-3W**, **2-3H$^+$-3W**, see Scheme 1 and Figures 1 and 2. The protonated complexes were calculated because the aniline N atoms of the ligands are easily protonated in acidic conditions and partially in aqueous solutions. The water molecules were added because (a) the M^{2+} cations can be coordinated with the solvent and (b) we wanted to include the solvent both explicitly and implicitly in the present calculations since it has been established that the augmentation of implicit solvent calculations with molecules of solvent is required in some cases, see for instance refs. [[35],[51–53]]. Here, the inclusion of coordinating solvent molecules explicitly has been done in accordance with the usual coordination number for each cation. The main coordination number of Ca^{2+} is 6, of Hg^{2+} is 2 and 3 and of Zn^{2+} is 4. The Ca^{2+} cation interacts with five atoms of AC, one nitrogen and four oxygen atoms, Hg^{2+} interacts with five atoms of DSC but mainly with two, and Zn^{2+} interacts with three atoms of DPA. Thus, for all three metal cations one water molecule is needed, attached to the metal. In the cases of **1-3W**, **1-M^{2+}-3W**, and **1-M^{2+}-3H$^+$-3W**, in the absence of a metal cation, the water molecules are added next to the ligands.

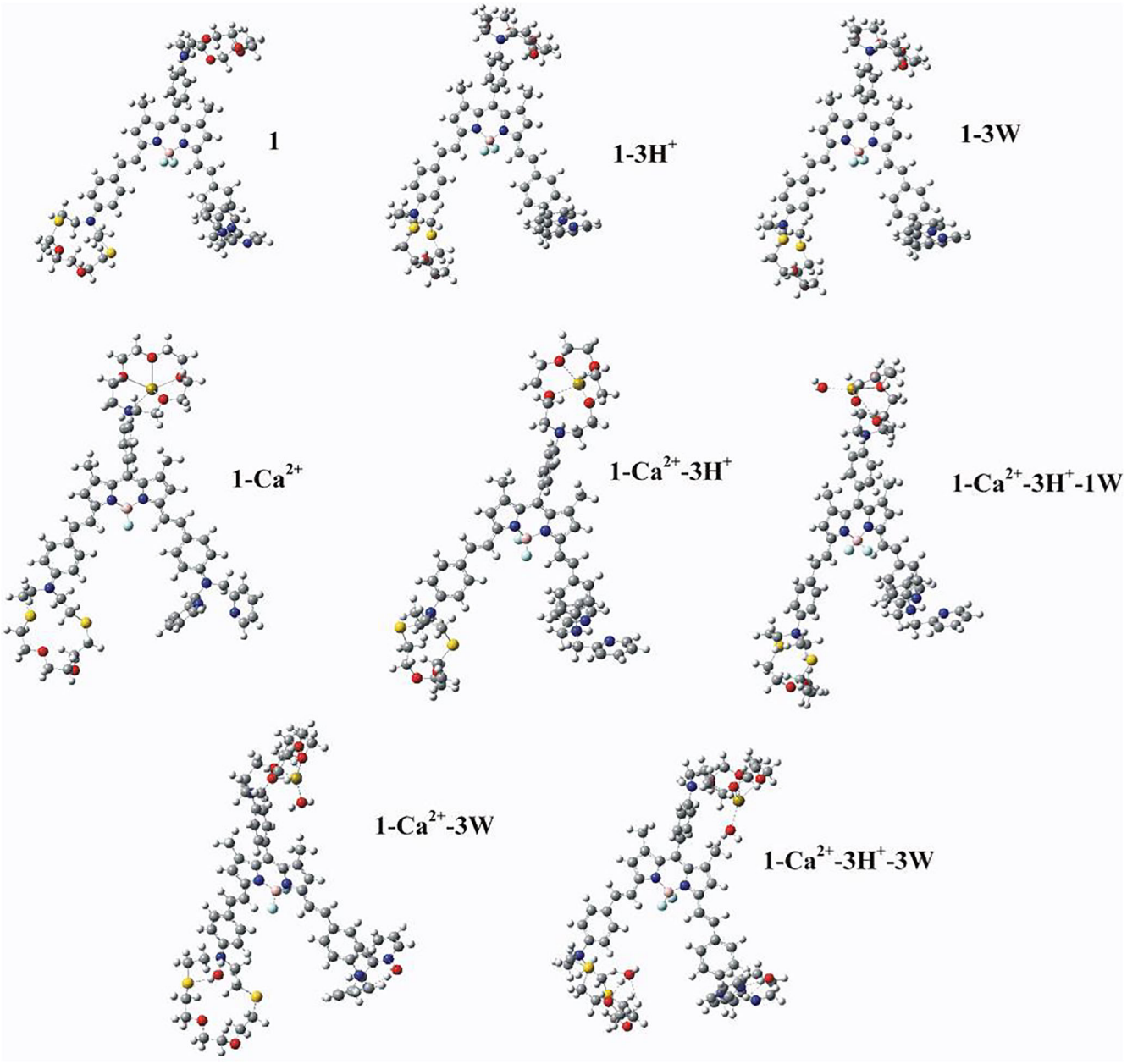

FIGURE 1 Calculated structures of the lowest in energy **1** and **1-Ca^{2+}** molecules, their protonated species and interacted species with 1 to 3 water molecules in water solvent

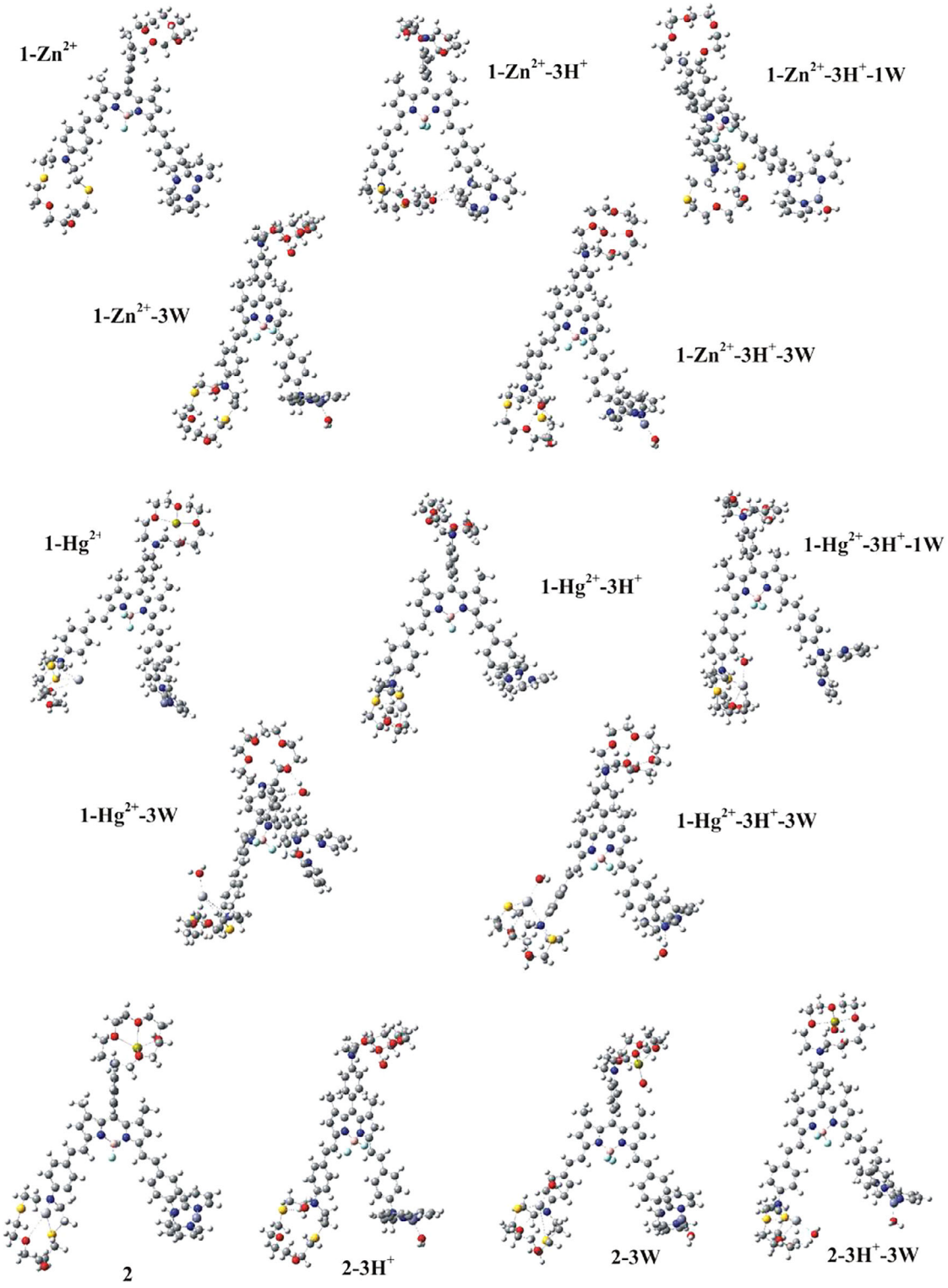

FIGURE 2 Calculated structures of the lowest in energy **1-Zn^{2+}**, **1-Hg^{2+}**, and **2** molecules, their protonated species and interacted species with 1 to 3 water molecules in water solvent

The PCM model is divided into a solute part lying inside a cavity, surrounded by the solvent part represented as a structureless material characterized by its macroscopic properties, that is, dielectric constants and solvent radius. It reproduces solvent effects usually well,[54] however, corrections to the calculated excitation energies for nonequilibrium solvent effects are required. Thus, the state-specific corrected linear response (cLR) approach,[55] is employed as described by Guido and Caprasecca.[55b]

In all cases, the absorption and the emission spectra of the studied systems were calculated including up to 30 singlet-spin excited electronic states, while within the cLR approach the spectra were calculated including three singlet-spin excited electronic states. Note that when including many singlet-spin excited electronic states in the cLR calculations, not only the calculations were time-consuming, but also in many cases the calculations were not converged. It should be noted that in some cases, some absorption maxima or emission maxima were affected by the number of calculated singlet states affects, probably due to convergence problems. For that reason, the spectra were calculated using various number of singlet states for validation. It should be noted that the emission spectra of **2-3H$^+$** and **2-3H$^+$-3W** species calculated via the B3LYP[56] functional because the PBE0 geometry optimization calculations do not converged. Note both PBE0 and B3LYP functionals predict similar data on **1**, **1-M^{2+}**, and **2** in acetonitrile solvent.[35]

All calculations were performed using the Gaussian 16 program package.[57] The coordinates of all the optimum structures are included in the accompanying supporting information (SI).

3 | RESULTS AND DISCUSSION

3.1 | Geometry

Complexation of the three metals, protonation, and complexation with water molecules of **1** result in geometry changes of its structure in the ground (Figures 1 and 2) and in the excited states which are critical for the fluorescent properties, see below. Selected geometries of the ground states (S_0) of lowest in energy conformations are given in Table 1, while selected geometries of other conformations, as also of the two excited states (S_1 and S_2) are given in Table 1S of SI along with the cartesian coordinates in Table 7S in SI.

In the ground (S_0) state, the range of the calculated bond distances between the metals and the ligating atoms in **2** are 2.48 to 2.9 Å for Ca^{2+}, 1.98 to 2.19 Å for Zn^{2+}, and 2.83 to 4.34 Å for Hg^{2+}, in water solvent. There are differences up to ±0.3 Å comparing with the corresponding

TABLE 1 Dihedral angles (°), N-H$^+$ bond distances (Å) and M…OH$_2$ bond distances (Å) of **1**, **1-Ca^{2+}**, **1-Zn^{2+}**, **1-Hg^{2+}**, and **2** species in S_0 state of the lowest in energy minima structures at the PBE0\6−31G(d,p)$_{H,C,O,N,S,Ca,Zn}$LANL2TZ$_{Hg}$ level of theory

Compound	C1NC2C3 AC	C4NC5C6 DSC	C7NC8C9 DPA	N-H AC	N-H DSC	N-H DPA	M^{2+}…OH$_2$[a]
1	161.8	169.8	127.7				
1-3W	160.5	168.6	136.8				
1-3H$^+$	129.3	130.5	130.5	1.032	1.041	1.047	
1-Ca^{2+}	127.2	169.3	178.4				
1-Ca^{2+}-3W	156.6	168.4	129.9				2.435
1-Ca^{2+}-3H$^+$	127.0	132.0	130.6	1.026	1.040	1.047	
1-Ca^{2+}-3H$^+$-1W	129.1	133.4	130.6	1.023	1.034	1.047	2.423
1-Ca^{2+}-3H$^+$-3W	139.4	139.8	131.5	1.023	1.021	1.024	2.432
1-Zn^{2+}	161.6	170.0	126.3				
1-Zn^{2+}-3W	166.5	155.6	127.9				2.035
1-Zn^{2+}-3H$^+$	129.9	131.7	129.6	1.031	1.039	1.024	
1-Zn^{2+}-3H$^+$-W	128.6	133.1	129.3	1.032	1.033	1.025	1.993
1-Zn^{2+}-3H$^+$-3W	131.5	131.3	139.4	1.024	1.025	1.024	1.975
1-Hg^{2+}	161.4	145.5	179.4				
1-Hg^{2+}-3W	173.0	165.7	176.4				2.572
1-Hg^{2+}-3H$^+$	129.3	133.8	130.4	1.032	1.036	1.047	
1-Hg^{2+}-3H$^+$-W	129.7	135.1	129.9	1.037	1.036	1.056	2.510
1-Hg^{2+}-3H$^+$-3W	130.5	137.3	139.8	1.024	1.024	1.022	2.507
2	127.1	145.4	127.3				
2-3W	126.9	143.1	129.0				2.444, 2.491, 2.057
2-3H$^+$	128.9	134.5	129.2	1.025	1.035	1.025	
2-3H$^+$-3W	130.0	134.3	130.6	1.025	1.037	1.025	2.424, 2.709, 1.968

[a]For **2** complex, the ordering of the M…OH$_2$ bond distances is Ca^{2+}…OH$_2$, Hg^{2+}…OH$_2$, Zn^{2+}…OH$_2$.

values in acetonitrile solvent. In **1-M^{2+}**, the bond distances between the metals and the ligating atoms are similar with those in **2**. Complexation of water molecules with the metals results only in small differences of the bond distances between the metals and the ligating atoms, that is, smaller than 0.1 Å. However, protonation of the aniline nitrogen atom results in differences up to 0.5 Å for the bond distances with the exception of aniline nitrogen atoms, where some of the bond distances are increased by up to 1.6 Å for DSC and DPA and up to 2 Å for AC for **1-M^{2+}** and **2**, see SI. It should be noted that regarding the relative position of the proton attached to aniline nitrogen atoms, various conformations of protonated species were calculated. It is interesting that the lowest in energy structures have the proton inside the crown of AC and DSC and in the cavity of DPA, both in free of metals **1** and in the complexed species. The structures having the proton out of the crown or out of the cavity (see close-up Figure 3) have N-H bond distances of 1.02 Å and they are lying 0.2 to 1 eV higher in energy than the structures having the proton inside the AC, DSC, and DPA groups, see Table 1S of SI. This occurs because the proton is further stabilized by the van der Waals interaction with S, O and N atoms inside the cavity. In order this interaction to be increased; the N-H distance is slightly elongated on the average by about 0.02 Å. The H-N bond distances, of the lowest in energy structure, are 1.032 (AC), 1.041 (DSC) and 1.047 Å (DPA) in **1-3H^{+}**, while they are decreased by 0.01 to 0.02 Å when the metals are complexed to ligands given that the S, O and N atoms inside the cavity interact mainly with the metals and not with the proton of the N aniline atom. In the calculated structures complexed with one or three water molecules, the water molecule was complexed to the metal atoms, while in absence of the metals, the water molecules were located next to the ligands forming van der Walls bonds. The M^{2+}…OH_2 bond distances range from 1.98(Zn) to 2.71(Hg) Å, see Table 1.

It is well known that the electron-donation by a tetrahedral N leads to a quasi-planar geometry at N.[58–61] Thus, it is of interest to consider the geometry at the N atoms of the ligands in the ground and the two lowest excited states, that is, whether it is a tetrahedral or a planar N atom approaching the geometry of quaternary N cation, and how it changes when the species are protonated or complexed with water. We observe that the geometry at the N atoms of the ligands is affected slightly by the change of solvent from acetonitrile to water when it is added implicitly, that is, up to 2° with the exception of the geometry at N of the DSC in **2** which changes up to 10°. However, the protonation or the complexation with water solvent affects significantly the N geometry resulting in changes of the geometry of the ligands and of their relative position with respect to the styryl-bodipy, see Figures 1 and 2. In detail, the protonation results in all N atoms being tetrahedral, while, the complexation changes it from tetrahedral to planar and vice versa. Additionally, the complexation of one metal cation affects the geometry not only of the corresponding ligand but also the geometry of the other two ligands. For instance, complexation of Ca^{2+} at the AC ligand or Hg^{2+} at DSC affects the geometry at N of DPA, which becomes planar compared to its tetrahedral geometry in **1**.

Within implicit inclusion of water solvent, for all calculated structures, in the ground state (S_0) and in the two lowest excited states (S_1 and S_2), of the uncomplexed **1**, the aniline N atom of the DPA ligand is nearly tetrahedral (128°), while the geometry at N of the other two ligands, that is, AC and DSC, is nearly planar (161-174°), see Table 1. Upon complexation by metal dications the geometry at N changes: the N atom in the AC ligand is tetrahedral in **1-Ca^{2+}** and **2**, while in **1-Zn^{2+}** and **1-Hg^{2+}**, it is quasi-planar as in **1**. In the DSC ligand, the N atom is quasi-planar in **1-Ca^{2+}**, **1-Zn^{2+}**, as in **1**; while in **2** and **1-Hg^{2+}** the dihedral angle is 145°. Finally, in the DPA ligand, the N atom is planar in **1-Ca^{2+}** and **1-Hg^{2+}** with a $C_7NC_8C_9$ dihedral angle of about 178°, while in **2** and **1-Zn^{2+}**, as also in **1**, it is tetrahedral. Thus, by the implicit inclusion of the water solvent, while in **1** only the N in DPA ligand is tetrahedral and the N atoms in the other two ligands are quasi-planar, in **2** all N atoms of the three ligands are nearly tetrahedral. Note that similar geometries were found previously in implicit inclusion of the acetonitrile solvent[35] or in the gas phase.[35]

Additionally to the implicit water solvent, the explicit inclusion of water by including three water molecules, each one in each ligand, affect the geometry of the aniline N atoms in the S_0 state, and in some species affect it drastically. For instance in **1-Ca^{2+}-3W** comparing to **1-Ca^{2+}**, where the water solvent is only implicitly included, the $C_1NC_2C_3$ dihedral angle of AC is increased by 39° namely, from 127° (**1-Ca^{2+}**) which is a tetrahedral geometry to 156° (**1-Ca^{2+}-3W**), while the $C_7NC_8C_9$ dihedral angle change from planar (178°) to tetrahedral (130°), see Table 1. In **1-Hg^{2+}-3W** and **1-Zn^{2+}-3W**, the N dihedral angles change up to 20° due to explicit inclusion of water; the biggest differences is observed in $C_4NC_5C_6$ dihedral angle of DSC from 170 (**1-Zn^{2+}**) to 156 (**1-Zn^{2+}-3W**) and from 146 (**1-Hg^{2+}**) to 166 (**1-Hg^{2+}-3W**). In **1-3W** and **2-3W** the

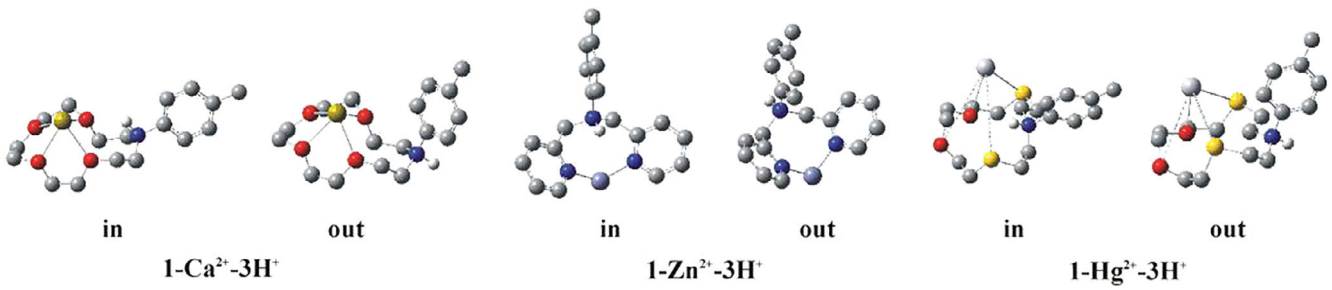

FIGURE 3 Close-up structures of in and out structures of protonated **1-M^{2+}-3H^{+}** species depicting only the hydrogen atom attached to anile N atom for clarity

differences, comparing to **1** and **2**, are smaller namely, 9 and 2°, respectively. Note that in **1-3W** the water molecules interact with the ligands via van der Waals bonds, while in **2-3W** the water molecules are complexed to the metals. Finally it should be noted that in **2**, the complexation of water in metals does not change the geometry of aniline N atoms.

In acidic conditions, the aniline N atoms will be protonated. This protonation leads to all aniline N atoms being tetrahedral in the ground state and two lowest excited states. The $C_1NC_2C_3$, $C_4NC_5C_6$, and $C_7NC_8C_9$ dihedral angle ranges from 127 to 134 in **1-3H$^+$**, **1-M^{2+}-3H$^+$**, and **2-3H$^+$** meaning that in all five calculated species have similar aniline N geometry with unprotonated **2**, see Table 1. Note, that in all calculated conformations of **1-3H$^+$**, **1-M^{2+}-3H$^+$**, and **2-3H$^+$**, and not only in the lowest ones presented in Table 1, the aniline N atoms are tetrahedral, see Table 1S of SI.

Furthermore, addition of explicit water molecules to the protonated species, which are complexed with the metal dications or they are attached via van der Waals bonds to the free ligands, result in the retaining of the tetrahedral geometry of the N aniline atoms. The tetrahedral $C_1NC_2C_3$, $C_4NC_5C_6$, and $C_7NC_8C_9$ dihedral angles change up to 2° in **1-M^{2+}-3H$^+$-1W**, and **2-3H$^+$-3W** comparing to **1-1-M^{2+}-3H$^+$**, and **2-3H$^+$** for all three S_0, S_1, and S_2 calculated states, while further addition of two water molecules attached to uncomplexed ligands results in an increase up to 10°, in the aniline dihedral angles of **1-M^{2+}-3H$^+$-3W** comparing to **1-M^{2+}-3H$^+$-1W**, that is, these dihedral angles range from 130° to 140°.

Note, that in all cases, for a specific species, that is, protonated or not, complexed or uncomplexed with metals and water, the geometries of the aniline N atom of all three ligands are similar, namely they remain tetrahedral or remain planar in all three calculated states (S_0, S_1, and S_2). The biggest calculated difference observed is 14° in $C_1NC_2C_3$ of AC in **1** between S_1 and S_2 states.

Thus, the N atoms of the three ligands change from tetrahedral to quasi-planar according to (a) the solvent, (b) acidity, and (c) which metal cation is added, that is, the complexation of the Ca^{2+} or Hg^{2+} in one ligand affects the geometry of the aniline N atoms of the ligands which are uncomplexed, while the addition of Zn^{2+} does not affect the properties of the other ligands. Thus, all these three factors change the electron-donating ability of the complexed or the uncomplexed ligands within the styryl-bodipy derivative.

3.2 | Spectra, energetics, and molecular orbitals

3.2.1 | Energetics

All species were fully geometry optimized in the ground state (S_0), in the two lowest singlet excited state. The vertical and adiabatic excitation energies with respect to the ground state and the corresponding corrected values with respect to the cLR approach are shown in Table 2. The two lowest excited states correspond to an emitting state and in a CT state. Including the water solvent implicitly, we observe that in **1** and **1-Zn^{2+}**, the lowest state is an emitting state, but the inclusion of the cLR approach reverse this ordering resulting in being the CT as the lowest one and so as the emission to be quenched. In **1-Ca^{2+}**, the lowest state is an emitting state both with and without the cLR approach. The attachment of a

TABLE 2 Vertical and adiabatic excitation energies (corrected values with respect to cLR approach) in eV of the two lowest excited states at the PBE0/6−31G(d,p)$_{H,C,O,N,S,Ca,Zn}$ LANL2TZ$_{Hg}$ level of theory

Compound	$S_0 \rightarrow S_{em}$ Vert	$S_0 \rightarrow S_{CT}$ Vert	$S_{em} \rightarrow S_0$ Vert	$S_{CT} \rightarrow S_0$ Vert	$S_0 \rightarrow S_{em}$ Adiab	$S_0 \rightarrow S_{CT}$ Adiab
1	1.98 (2.06)	2.20 (2.20)	1.62 (1.91)	1.83 (1.26)	1.71 (1.99)	2.00 (1.43)
1-3H$^+$_a	2.15 (2.25)	3.17 (3.17)	1.74 (2.08)	2.87 (2.88)	1.84 (2.17)	3.02 (3.02)
1-Ca^{2+}	1.85 (1.93)	2.41 (2.50)	1.52 (1.78) (1.79)	2.27 (2.24) (1.43)	1.59 (1.86) (1.95[a])	2.33 (2.30) (1.61[a])
1-Ca^{2+}-3H$^+$	1.14 (2.24)	3.16 (3.17)	1.74 (2.08)	2.86 (2.87)	1.83 (2.17)	3.05 (3.06)
1-Ca^{2+}-3H$^+$-1W	2.15 (2.25)	3.17 (3.18)	1.75 (2.08)	2.88 (2.88)	1.84 (2.18)	3.00 (3.00)
1-Zn^{2+}	1.97 (2.04)	2.14 (2.14)	1.61 (1.87)	1.60 (1.21)	1.69 (1.96)	1.70 (1.31)
1-Zn^{2+}-3H$^+$	2.17 (2.27)	2.69 (2.69)	1.77 (2.08)	2.10	1.87 (2.18)	2.37
1-Zn^{2+}-3H$^+$-1W	2.15 (2.25)	2.76 (2.76)	1.74 (2.07)	2.16	1.83 (2.17)	2.49
1-Hg^{2+}	1.91 (1.99)	2.06 (2.06)	1.57 (1.85)	1.58 (1.24)	1.66 (1.93)	1.65 (1.55)
1-Hg^{2+}-3H$^+$	2.15 (2.25)	2.65 (2.65)	1.75 (2.08)	2.33	1.84 (2.18)	2.45
1-Hg^{2+}-3H$^+$-1W	2.18 (2.28)	2.84 (2.84)	1.77 (2.10)	2.29	1.87 (2.20)	2.43
2	2.15 (2.24)	2.24 (2.34)	1.91 (2.00)	1.88 (2.08)	1.90 (2.16)	2.20 (2.30)
2-3H$^+$[b]	2.04 (2.22)	2.69	1.69 (1.99)	1.75	1.99	2.30

[a]In **1-Ca^{2+}-1W**.
[b]B3LYP/6−31G(d,p)$_{H,C,O,N,S,Ca,Zn}$ LANL2TZ$_{Hg}$ values.

water molecule reverses the ordering, making the CT as the lowest one. In **1-Hg^{2+}** the two lowest states are energetically degenerate, while in **2** the emitting state is the lowest one. In acidic conditions, the protonation of the aniline N atom results in an increase of about 0.2 eV to higher energy for the first excited state and an increase that range from 0.3 (**2-3H^{+}**) to 1.6 (**1-3H^{+}**) eV for the CT state. As a result, in all cases the CT state is the second excited state and all five species emit at about 2.2 eV. The addition of the explicit water solvent in the protonated species, only slightly affects the emission by up to 0.04 (0.01) eV without (with) the cLR approach.

The above conclusions for the unprotonated species in water solvent are in accordance with those in acetonitrile solvent,[35] where, it was also found that the observed quenching of emission of **1** and **1-M^{2+}** may be attributed to the fact that their first excited state is a charge-transfer (CT) state whereas this does not happen for the complex **2**. Similarly, for the correct ordering of the excited states, the cLR approach was required; while in the case of **1-Ca^{2+}**, the additional explicit inclusion of the solvent was necessary for the quenching of the emission spectra. These conclusions were in agreement with experiment where an intense emission peak only for **2** was observed in acetonitrile solvent.[12] The results obtained by the two solvents differ only in the position of the CT states. Within the cLR approach, in water solvent they are red shifted by about 0.3 eV compared to acetonitrile solvent. The positions of the emitting states in both solvents are similar.

It should be noted that in water solvent a very small portion of **1**, **1-M^{2+}** and **2** will react reversibly with water resulting in protonation of aniline N atoms. All these protonated species, as mentioned above, have the emitting state as the lowest one, while their CT state is shifted in higher energies; the energy difference between these two states is about 1 eV. As a result, all protonated species will emit. However, their portion comparing to unprotonated species is very small, and as a result, the styryl-bodipy derivative will behave similarly to acetonitrile solvent, **2** will present an intense emission peak while **1**, **1-M^{2+}** may present a weak peak. On the contrary, in acidic conditions all five **1**, **1-M^{2+}** and **2** species will present an intense emission peak.

3.2.2 | Spectra

The absorption vertical excitation energies $S_0 \rightarrow S_x$ and the emission energies $S_x \rightarrow S_0$ of the two lowest excited states, their *f*-values, their main excitations and corresponding coefficients for the unprotonated, protonated, complexed with water, complexed with a metal cation or with three metal cations of styryl-bodipy derivative in water solvent, including it also explicitly, are collected in Tables 3 and 4 and in Tables 4S and 5S of the SI. The absorption and emission spectra are depicted Figures 1S-2S of SI and the relative absorbance spectra are depicted in Figure 4.

TABLE 3 Absorption maxima, λ_{max} (nm), of $S_0 \rightarrow S_x$, *f*-values for absorption, of protonated, unprotonated, complexed with water of **1**, **1-M^{2+}**, and **2** in water solvent at the PBE0/6–31G(d,p)$_{H,C,O,N,S,Ca,Zn}$ LANL2TZ$_{Hg}$ level of theory

Compound		1		1-Ca^{2+}		1-Zn^{2+}		1-Hg^{2+}		2	
		λ_{max}	*f*	λ_{max}	*f*	λ_{max}	*f*	λ_{max}	*f*	λ_{max}	*f*
	S_1	624.9 (601.5)	1.1518	669.7 (643.3)	1.0915	629.2 (606.7)	1.1364	646.2 (622.1)	1.0549	575.5 (552.7)	1.1161
	S_2	564.8[a]	0.0525	496.3	0.7355	579.6[a]	0.0479	600.8[a]	0.0014	553.8[a]	0.0038
	S_3	464.2	0.7923	402.2	0.0710	393.4[b]	1.1761	557.2[a]	0.1488	454.9	0.7632
	S_4	382.4	1.1959	388.7	1.5984			486.6	0.9547	369.7[c]	0.7372
	S_8							386.8	1.5757	342.9[d]	0.8120
-3H^{+}	S_1	577.2 (550.8)	1.0801	579.3 (552.5)	1.0810	570.7 (547.2)	0.8668	577.6 (551.1)	1.0963	608.4 (559.0)	1.2927
	S_2	391.6[a]	0.0127	392.1	0.0407	461.2[a]	0.0010	467.4[a]	0.0001	460.7[a]	0.0001
	S_3	380.7[a]	0.0348	382.2[a]	0.0626	368.9	1.6592	391.0[a]	0.0005	357.9[e]	1.9056
	S_5	368.6	1.3574	373.0	2.2965			372.3	2.4130		
-3H^{+}-*x*W[f]	S_1			577.6 (550.7)	1.1139	578.0 (551.3)	1.1278	569.7 (544.4)	1.0574	623.4 (562.5)[g]	1.1004
	S_2			390.9[a]	0.0162	449.5[a]	0.0010	437.2[a]	0.0001		
	S_3			380.2[a]	0.0314	373.2[b]	1.7084	385.9[a]	0.0055		
	S_4			372.9	2.1391			368.7[h]	2.4249		

Note: In parenthesis are given the values within the cLR approach.
[a]CT states.
[b]S_6.
[c]S_{10}.
[d]S_{12}.
[e]S_7.
[f]*x* = 1 for **1-M^{2+}-3H^{+}-1W**, and *x* = 3 for **2-3H^{+}-3W**.
[g]B3LYP/6–31G(d,p)$_{H,C,O,N,S,Ca,Zn}$ LANL2TZ$_{Hg}$ values.
[h]S_5.

TABLE 4 Emission maxima, λ_{max} (nm), of $S_x \rightarrow S_0$, f-values for absorption, of protonated, unprotonated, complexed with water of **1**, **1-M^{2+}**, and **2** in water solvent at the PBE0/6−31G(d,p)$_{H,C,O,N,S,Ca,Zn}$ LANL2TZ$_{Hg}$ level of theory

Compound		1		1-Ca^{2+}		1-Zn^{2+}		1-Hg^{2+}		2	
		λ_{max}	f	λ_{max}	f	λ_{max}	f	λ_{max}	f	λ_{max}	f
	S_1	763.8 (650.2)	1.3438	817.0 (694.9)[a]	1.2481	772.2 (661.9)	1.3254	787.6 (671.7)	1.2945	650.(620.6) (729.8[b])	1.2518
	S_2	676.9 (984.1)[c]	0.0002	547.0 (554.7)[a]	1.2375	594.5 (1023.2)[c]	0.1384	648.4 (1000)[c]	0.0020	624.9 (597.1)[c]	0.0341
-3H$^+$	S_1	710.9 (596.6)	1.3117	710.9 (596.1)	1.3012	700.8 (595.8)	1.1226	710.3 (595.7)	1.3113	735.8 (621.7)[d]	1.3088
	S_2	431.3 (430.9)[c]	0.0138	434.0 (432.2)[c]	0.2138	590.5[c]	0.0097	532.3[c]	0.0001	677.0 (589.1)[c,d]	0.0031
-3H$^+$-xW[e]	S_1			710.3 (595.4)	1.3211	712.9 (597.7)	1.3293	701.4 (591)	1.2791		
	S_2			430.6 (430.2)[c]	0.0120	573.4[c]	0.0243	541.1[c]	0.0002		

Note: In parenthesis are given the values with in the cLR approach.
[a]In **1-Ca^{2+}-1W**, S_{em}: 693 nm, S_{CT}: 869 nm within cLR approach.
[b]Including three singlet states.
[c]CT states.
[d]B3LYP/6−31G(d,p)$_{H,C,O,N,S,Ca,Zn}$ LANL2TZ$_{Hg}$ values.
[e]x = 1 for **1-M^{2+}-3H$^+$-1W**, and x = 3 for **2-3H$^+$-3W**.

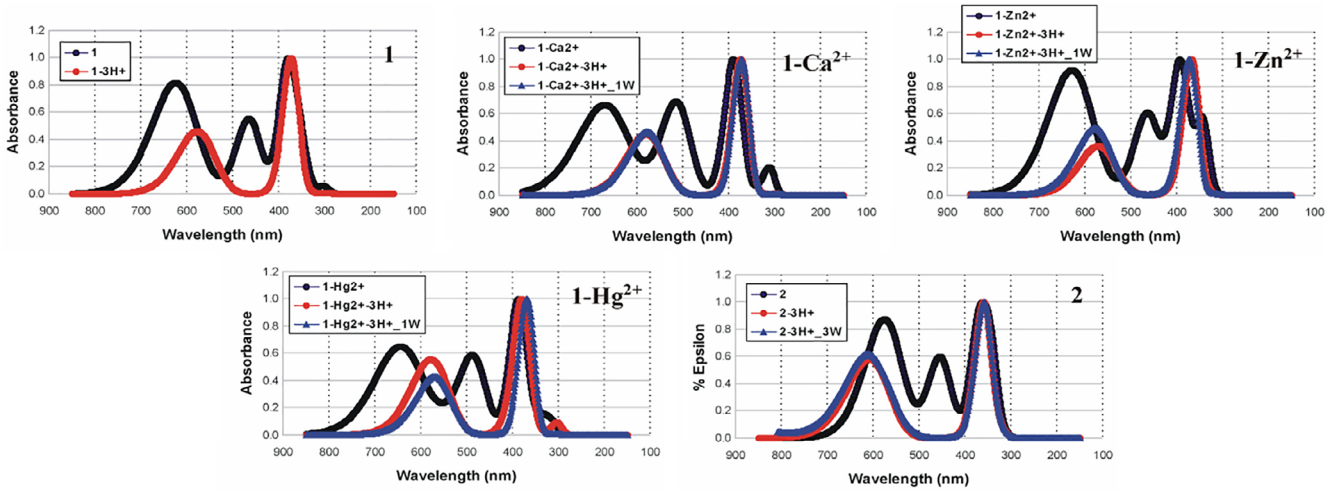

FIGURE 4 Relative absorbance spectra of the lowest in energy of **1**, **2**, **1-Ca^{2+}**, **1-Zn^{2+}**, and **1-Hg^{2+}**, their protonated species, and their protonated and complexed with water species in water solvent

Absorption spectra

The first calculated absorption λ_{max} values of **1**, **1-Ca^{2+}**, **1-Zn^{2+}**, and **1-Hg^{2+}** and **2** in water and in acetonitrile solvent[35] are almost the same in both solvents. In water solvent (acetonitrile solvent) are 625 (624), 670 (678), 629 (629), 646 (643), and 576 (577) nm, while the corresponding experimental values[12] in acetonitrile solvent are 692, 672, 668, 630, and 626 nm, see Table 3 and Table 4S of SI. The cLR approach, in both solvents, shifts only a little the absorption maxima, that is, by less than 0.1 eV. Thus, the shifts of the main absorption peaks with respect to the experimental values range from 0.02 to 0.20 eV, while including the cLR approach, the corresponding shifts range from 0.03 to 0.27 eV. Shifts of about 0.2 eV are considered as showing very good agreement between experiment and theory.[62,63]

The protonation of aniline N atoms results in a change of the general shape of absorption spectra for all five calculated species. In order to compare the absorption spectra of all calculated species, we plot the relative absorbance vs wavelength spectra, see Figure 4, where for each absorption spectrum, the epsilon values were divided by its epsilon maximum value. The absorption spectra of unprotonated species have three main peaks, while the corresponding spectra of protonated species or the protonated and complexed with water have two main peaks, see Figure 4. This is due to the fact that the second peak is significantly blue shifted next to the third peak and as a result the two main peaks are observed. Finally, for all three species protonated, unprotonated, complexed with water a peak at about 380 nm is observed with the same relative absorbance, see Figure 4.

In details, the protonation of aniline N atoms of **1**, **1-M^{2+}**, and **2** results in blue shifts in the first λ_{max} of about 50 (**1-3H$^+$**), 100 (**1-Ca^{2+}-3H$^+$**), 60 (**1-Zn^{2+}-3H$^+$**), 70 (**1-Hg^{2+}-3H$^+$**), and 50 nm (**2-3H$^+$**), that is, the **1-Ca^{2+}-3H$^+$** presents the largest shifts, see Table 3. Note that all calculated

singlet excited states present blue shifts under protonation; however, the largest blue shifts are observed for the second excited state, which is a CT state, up to 170 nm (**1**). The first absorption λ_{max} values range from 571 (**1-Zn^{2+}-3H^{+}**) to 608 (**2-3H^{+}**) nm, while the first CT states are located about at 390 for **1-3H^{+}** and **1-Ca^{2+}-3H^{+}** and at about 460 nm for **1-Zn^{2+}-3H^{+}**, **1-Hg^{2+}-3H^{+}** and **2-3H^{+}**, showing that the CT process is facilitated energetically by the presence of Zn^{2+} and Hg^{2+}. However, in general the protonation results in making more difficult energetically the CT process, see Table 3. Finally, further complexation of protonated **1-3H^{+}**, **1-M^{2+}-3H^{+}**, and **2-3H^{+}** species with water molecules, complexed with metals or attached to the uncomplexed ligands, results only in small blue or red shifts for all peaks. In the first λ_{max}, the shifts are up to 15 nm.

Emission spectra

The nonequilibrium solvation effects are substantial and as a result the cLR approach is necessary for the correct ordering of the excited state. For instance, while the optimization of the first two excited state of **1**, **1-Zn^{2+}** and **1-Hg^{2+}** resulted in an emitting state as the first excited state, and a CT state as the second one, the inclusion of the cLR process reverse the ordering. Thus, the CT state is the first one excited state and the emitting state is the second one. However, in the case of **1-Hg^{2+}**, within cLR approach, the energy difference between the CT state and the emitting state is rather big, 0.6 eV, and as in the case of acetonitrile solvent,[35] a weak peak is possible to be observed because the population of the second excited state (S_2) cannot be completely reduced by internal conversion, allowing some emission to be observed from S_2. In **1-Ca^{2+}** the optimization of its two lowest excited state resulted in two emitting states with and without the inclusion of the cLR process. However, the complexation of a water molecule with Ca^{2+} resulting in a CT state being the first one excited state and an emitting state being the second one. Finally, in **2** an emitting state is the first excited state and a CT state is the second one without and within cLR approach. Thus, we expect **2** to emit. The emission maximum was calculated at 650 (621) nm without(with) cLR approach, see Table 4. In acetonitrile solvent, the emission maximum was calculated at 649 (619) nm[35] without(with) the cLR approach, in excellent agreement with the experimental value of 656 nm.[12]

The protonation of the aniline N atoms results in being the emitting state the first excited state without or within cLR approach, see Table 4. The additional complexation of water solvent molecules to the metals or the attachment to the free ligands does not affect the spectra, that is, the emitting state remains the first excited state and the CT state is the second one without or within cLR approach. The **1-3H^{+}**, **1-Ca^{2+}-3H^{+}**,

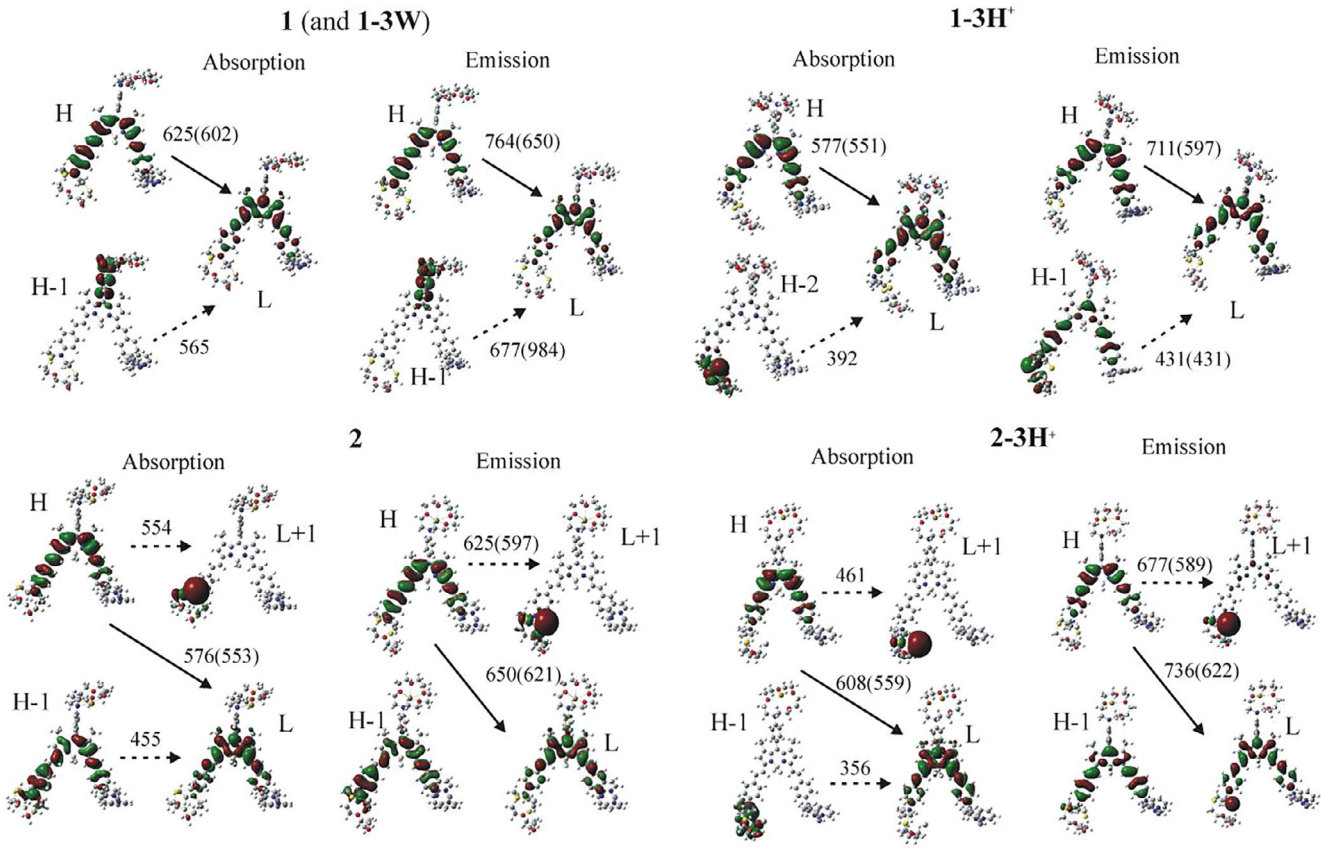

FIGURE 5 Electron density plots of the molecular orbitals involved in the excitations corresponding to the major peaks for transitions from the ground (S_0) to the two lowest excited states (S_1 and S_2) of the unprotonated and protonated **1** and **2**. The S_0 geometry (absorption) and the optimized geometry of the corresponding excited state (emission) are employed. λ_{max} in nm of the singlet excitations (solid arrows) and charge transfer excitations (dash arrows) are given without and (with inclusion of the cLR correction)

1-Zn^{2+}-3H^{+}, and **1-Hg^{2+}-3H^{+}** species have similar emission spectra, see Figure 2S of SI. All they emit at about 710 (600) nm, without (with) the cLR approach, see Table 4 and Table 5S of SI. It should be noted that emission of **2-3H^{+}** was optimized at B3LYP level of theory, because the optimization at PBE0 does not converge. B3LYP predicts emission at 736 (622) nm for **2-3H^{+}** larger than the values of **1-3H^{+}** and **1-M^{2+}-3H^{+}**, note that our previous study has shown that the B3LYP values are about 30 nm red shifted comparing to PBE0 values,[35] and as a result the emission at 736 (622) nm of **2-2H^{+}** at B3LYP level is consistent with the values of 710 (600) nm of **1-3H^{+}** and **1-M^{2+}-3H^{+}**.

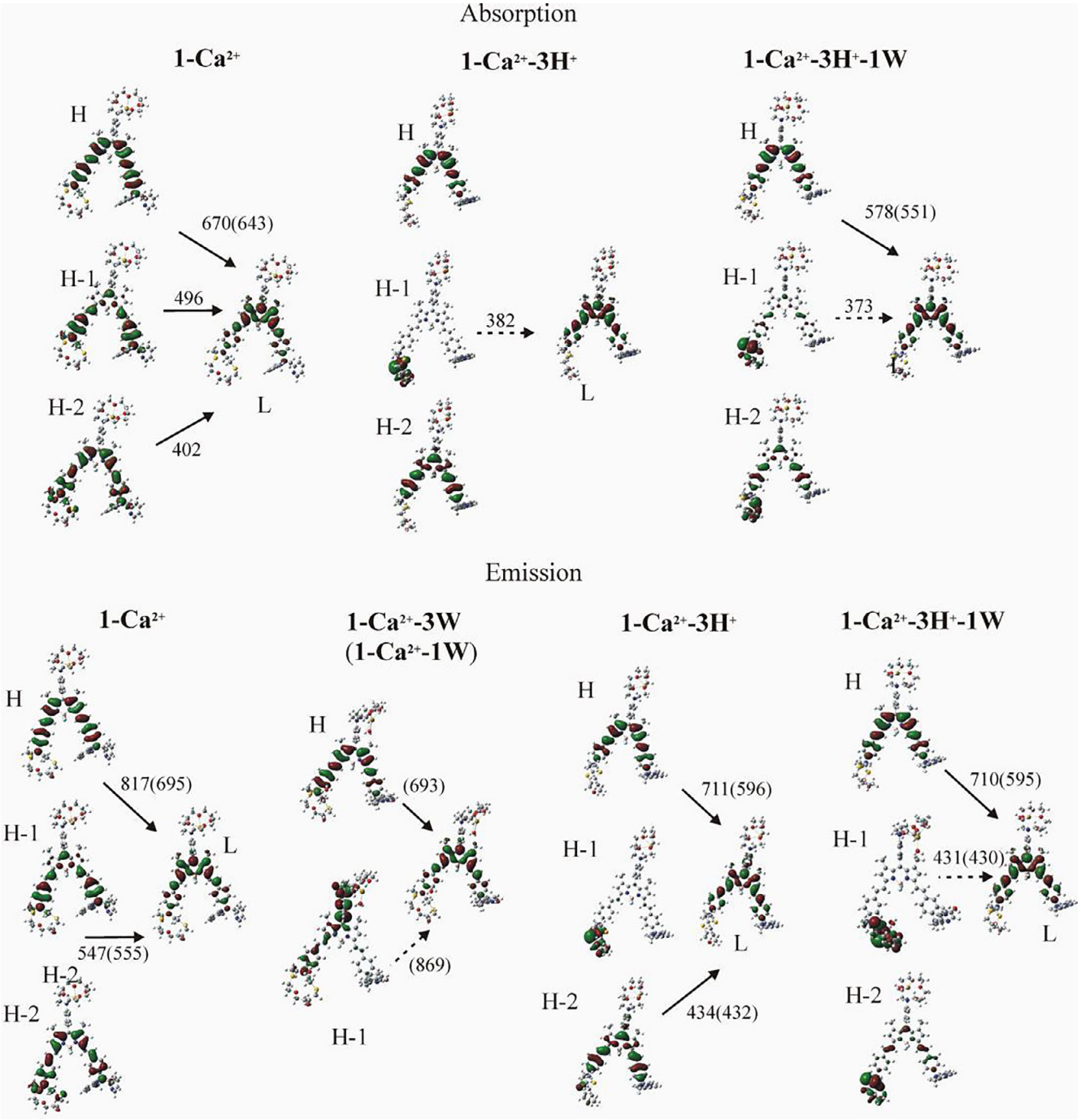

FIGURE 6 Electron density plots of the molecular orbitals involved in the excitations corresponding to the major peaks for transitions from the ground (S_0) to the two lowest excited states (S_1 and S_2) of the unprotonated and protonated, complexed and uncomplexed with water molecules **1-Ca^{2+}**. The S_0 geometry (absorption) and the optimized geometry of the corresponding excited state (emission) are employed. λ_{max} in nm of the singlet excitations (solid arrows) and charge transfer excitations (dash arrows) are given without and (with inclusion of the cLR correction)

This study shows that the key factor for the emission is the simultaneous tetrahedral geometry of all three aniline N atoms, that is, the emission is regardless of the metal dications complexation. Thus, in acidic conditions this is accomplished via the existence of protons, while in acetonitrile solvent via the existence of the three metal dications attached to the three different receptors.

3.2.3 | Molecular orbitals

In Figures 5–8 and Figures 3S-7S of SI the electron density plots of the HOMO (H), HOMO-1 (H-1), HOMO-2 (H-2), LUMO (L), and LUMO+1 (L + 1) molecular orbitals (MO) involved in the main singlet excitations from the ground state (S_0) to the two lowest excited states, at the S_0 geometry for absorption and at the S_1 and S_2 geometries for emission, are depicted. The H and L MO are the same for all five species unprotonated, protonated and/or complexed with water for the ground and the two excited states, that is, they are located on dipyrromethene and on two styrenes. For the H-2, H-1 and L + 1 MO, there are differences among all calculated species and different states, see Figures 5–8 and Figures 3S-7S of SI. In all species, the emitting state is an excitation within the dipyrromethene-two styrenes group.

Regarding the relative energy differences between MO (cf. Table 6S of SI), we observe that the energy difference between H and L MO (H-L) decreases up to 0.25 eV, while the H-(H-1) energy increases up to 0.14 eV in the S_1 comparing to S_0, for all calculated species, that is, unprotonated, protonated, complexed, uncomplexed with metals and/or water molecules, showing that both H-1 and L are stabilized in S_1 with respect to S_0. It should be noted that the protonation results in an increase of the H-L energy up to 0.28 eV and a significant decrease of the

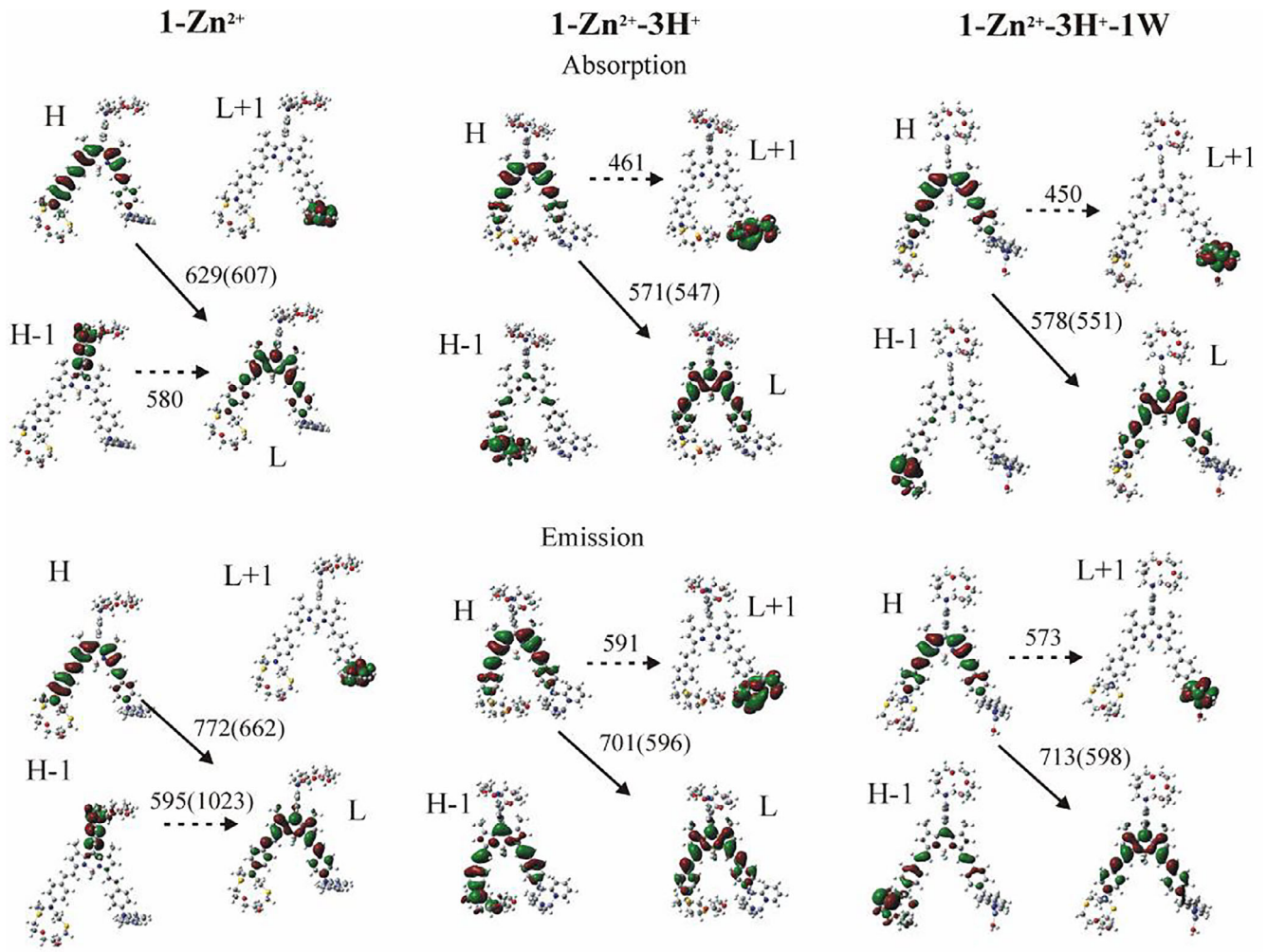

FIGURE 7 Electron density plots of the molecular orbitals involved in the excitations corresponding to the major peaks for transitions from the ground (S_0) to the two lowest excited states (S_1 and S_2) of the unprotonated and protonated, complexed and uncomplexed with water molecules **1-Zn^{2+}**. The S_0 geometry (absorption) and the optimized geometry of the corresponding excited state (emission) are employed. λ_{max} in nm of the singlet excitations (solid arrows) and charge transfer excitations (dash arrows) are given without and (with inclusion of the cLR correction)

H-(H-1) energy gap up to 0.78 eV in S_0, S_1, and S_2 comparing to the corresponding energy gaps in un- protonated species. Moreover, in the case only of the CT state, the H-(L + 1) energy gap is decreased up to 0.46 eV upon protonation. Thus, the H-1 MO is energetically stabilized, the L is destabilized, while the L + 1 is stabilized only in the CT state, which is expected. Finally, the water attachment or complexation to the protonated species, only slightly affects the MO energy gaps, and this is consistent with the fact that their spectra do not change upon complexation or attachment of water.

Regarding the CT excitation, the benzo-AC acts as an electron donor and the dipyrromethene-two styrenes group acts as an electron acceptor in **1**, **1-Zn^{2+}**, **1-Ca^{2+}-1W**, and **1-Hg^{2+}**. With the exception of **1-Ca^{2+}-1W**, the addition of explicit water molecules does not change the type of CT excitations. Moreover, in **2** and in the lowest CT state of **1-Hg^{2+}**, the benzo-AC acts as an electron donor, while the DSC-Hg^{2+} group acts as an electron acceptor. Thus, the ascending ordering of the groups with respect to the capability to attract electrons is benzoazacrown ether < dipyrromethene-two styrenes < DSC-Hg^{2+}.

It should be noted that upon protonation, in **1-3H^{+}**, **1-Ca^{2+}-3H^{+}** and **2-3H^{+}**, the DSC ligand is the electron donor and the dipyrromethene-two styrenes group is the electron acceptor. However, in **1-Hg^{2+}-3H^{+}** and in the lowest CT state of **2-3H^{+}**, the dipyrromethene-two styrenes group acts as an electron donor and DSC-Hg^{2+} as an electron acceptor. In **1-Zn^{2+}-3H^{+}** the dipyrromethene-two styrenes group acts as an electron donor and the DPA acts as an electron acceptor. Thus, in **1-3H^{+}**, **1-Ca^{2+}-3H^{+}**, and **1-Zn^{2+}-3H^{+}**, the protonation affects the type of the lowest in energy CT state, while in **2-3H^{+}** and **1-Hg^{2+}-3H^{+}**, the protonation does not affect it. It only affects the type of the second CT state, see Figures 5–8. The addition of explicit water molecules complexed to metal or attached to the ligands on unprotonated or protonated species do not change the type of the CT state, with exception of **1-Ca^{2+}** as mentioned above. Finally, the CT states in emission spectra are blue shifted comparing to absorption spectra, see Figures 5–8.

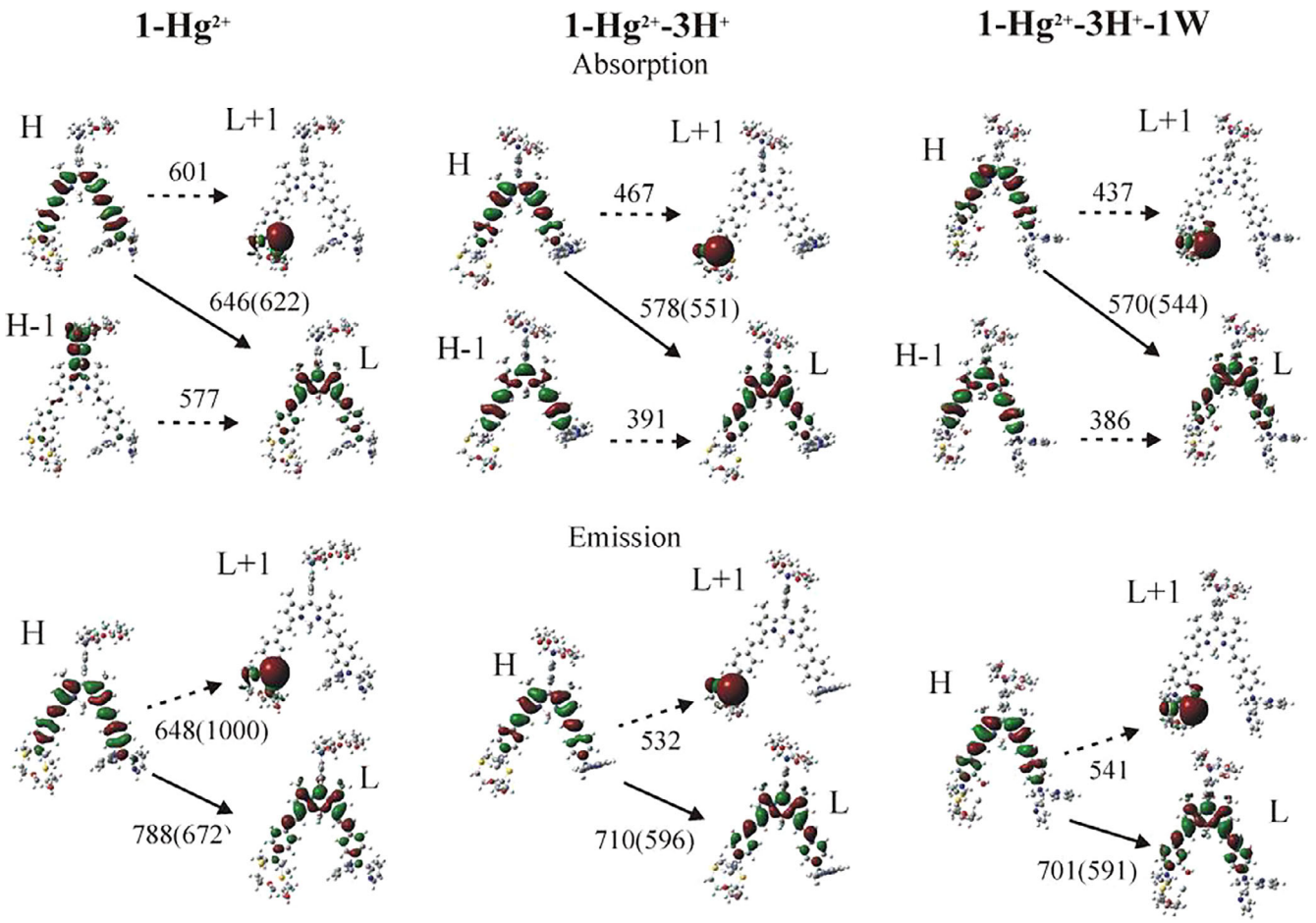

FIGURE 8 Electron density plots of the molecular orbitals involved in the excitations corresponding to the major peaks for transitions from the ground (S_0) to the two lowest excited states (S_1 and S_2) of the unprotonated and protonated, complexed and uncomplexed with water molecules **1-Hg^{2+}**. The S_0 geometry (absorption) and the optimized geometry of the corresponding excited state (emission) are employed. λ_{max} in nm of the singlet excitations (solid arrows) and charge transfer excitations (dash arrows) are given without and (with inclusion of the cLR correction)

TABLE 5 Emission spectra in acetonitrile solvent, in water solvent and in acidic condition in water solvent

	Acetonitrile	Water	Acidic conditions
1	No emit	A very weak peak	Emit
1-Ca^{2+}	No emit	A very weak peak	Emit
1-Zn^{2+}	No emit	A very weak peak	Emit
1-Hg^{2+}	A weak peak	A weak peak	Emit
2	Emit	Emit	Emit

To summarize, the bodipy system is connected with one PET active group (DPA) and two ICT active groups (DSC and AC). The PET activity is linked to the presence of a DPA ligand-centered orbital above the bodipy-centered orbital, while the ICT activity is linked to the presence of a DSC or AC ligand-centered orbital. Note that the ICT activity of DSC acts antagonistic to the ICT activity of AC and the PET activity of DPA. The emission in all five calculated species protonated or unprotonated is from an orbital that is mainly a bodipy-centered H orbital, to the L orbital, which is also mainly dye centered. Regarding the CT state of the unprotonated **1**, **1-Ca^{2+}** and **1-Zn^{2+}** species, the CT state comes from the AC ligand-centered orbital to bodipy-centered orbital. On the contrary, upon protonation the CT state is from DSC to bodipy-centered orbital for **1** and **1-Ca^{2+}** species, and from mainly bodipy-centered H orbital to DPA-Zn orbital which becomes the L orbital. Thus, the ICT activity is the dominant one for **1**, **1-3H^{+}**, **1-Ca^{2+}**, **1-Ca^{2+}-3H^{+}** and **1-Zn^{2+}** species, while the PET activity is the dominant one for **1-Zn^{2+}-1W**. The complexation of the Hg^{2+} metal results in a change of the character of the CT state of **1**, regardless to the protonation, that is, the transfer occurs from a mainly bodipy-centered H orbital to DSC-Hg orbital L orbital for both unprotonated and protonated **1-Hg^{2+}** and **2**.

4 | SUMMARY AND CONCLUSIONS

It has been found theoretically by our group,[35] and experimentally by Bozdemir et al[12] that the styryl-bodipy derivative **1** can act as a three metal-cation-receptor fluorophore and as a three input AND molecular logic gate in acetonitrile solvent, because only **2** emits, while in **1** and **1-M^{2+}**, the emission is quenched due to the fact that their first excited state is a charge-transfer (CT) state whereas this does not happen for the complex **2**. Here, we study theoretically the photophysical processes of a styryl-bodipy derivative (**1**) of its monometallic complexes **1-M^{2+}** (M = Ca, Zn, and Hg), and its trimetallic complex (**2**) unprotonated, protonated and/or complexed with water molecules in water solvent and in acidic conditions via DFT and TDDFT calculations. The cLR correction to the energies for nonequilibrium solvent effects is also included.

The absorption spectra of **1**, **1-M^{2+}** and **2** are almost the same in acetonitrile and water solvent, while the protonation of aniline N atoms of **1**, **1-M^{2+}**, and **2** results in red shifts in the first λ_{max} of about 50 (**1-3H^{+}**), 100 (**1-Ca^{2+}-3H^{+}**), 60 (**1-Zn^{2+}-3H^{+}**), 70 (**1-Hg^{2+}-3H^{+}**), and 50 nm (**2-3H^{+}**).

Regarding the emission spectra, for the correct ordering of the excited states, the inclusion of corrections to the excitation energies for non-equilibrium solvent effects is required as well as the explicit inclusion of the solvent in the case of **1-Ca^{2+}**. In **1** and **1-M^{2+}** the first excited state is a CT state, while in **2** the excited state is an emitting state. The protonation of the aniline N atoms results in being the emitting state the first excited state in all species. The additional complexation of water solvent molecules to the metals or the attachment to the free ligands does not affect the spectra.

Thus, in acidic conditions, where the aniline N atoms of the three ligands are protonated, all five species will emit at about 600 nm (orange area). On the contrary, in water solvent as well in acetonitrile solvent there will be a quenching of emission spectra in **1** and **1-M^{2+}** and a retaining in **2**. However, contrary to acetonitrile solvent, for **1** and **1-M^{2+}** in water solvent a weak peak will be observed due to the occurrence of a small ratio of reversible protonation. Our conclusions are summarized in Table 5.

To sum up, the emission is accomplished by the simultaneous tetrahedral geometry of all three aniline N atoms. In acidic conditions, this is fulfilled by the existence of protons, while in acetonitrile or water solvent this is achieved via the existence of the three metal dications attached to the three different receptors.

Regarding the possibility of MLG action, the results show that while **1** remains a three input AND molecular logic gate if the solvent is changed from acetonitrile to water, in acetonitrile **1** acts as a better MLG candidate. However, the MLG action is not retained in acidic conditions.

ACKNOWLEDGMENTS

We acknowledge support of this work by the projects: (a) “Advanced Materials and Devices” (MIS 5002409) which is implemented under the “Action for the Strategic Development on the Research and Technological Sector” and (b) “National Infrastructure in Nanotechnology, Advanced Materials and Micro-/Nanoelectronics” (MIS 5002772) which is implemented under the action “Reinforcement of the Research and Innovation Infrastructure”, funded by the Operational Programme “Competitiveness, Entrepreneurship and Innovation” (NSRF 2014-2020) and cofinanced by Greece and the European Union (European Regional Development Fund).

ORCID

Demeter Tzeli https://orcid.org/0000-0003-0899-7282

REFERENCES

[1] P. de Silva, H. Q. N. Gunaratne, C. P. McCoy, *Nature* **1993**, *364*, 42.
[2] A. P. de Silva, H. Q. N. Gunaratne, T. Gunnlaugsson, A. J. M. Huxley, C. P. McCoy, J. T. Rademacher, T. R. Rice, *Chem. Rev.* **1997**, *97*, 1515.
[3] B. Valeur, *Molecular Fluorescence*, Wiley, Weiheim **2002**.
[4] K. Rurack, U. Resch-Genger, *Chem. Soc. Rev.* **2002**, *31*, 116.
[5] K. Szacilowski, *Chem. Rev.* **2008**, *108*, 3481.
[6] S. Ozlem, E. U. Akkaya, *J. Am. Chem. Soc.* **2009**, *131*, 48.
[7] D. C. Magri, A. P. de Silva, *New J. Chem.* **2010**, *34*, 476.
[8] J. Ling, B. Daly, V. A. D. Silverson, A. P. de Silva, *Chem. Commun.* **2015**, *51*, 8403 and references therein.
[9] G. T. Yan, H. Li, Y. R. Zhu, B.-B. Shi, W. Qu, Q. Lin, H. Yao, Y.-M. Zhang, T.-B. Wei, *New J. Chem.* **2015**, *39*, 8797.
[10] S. Karmakar, S. Mardanya, S. Das, S. Baitalik, *J. Phys. Chem. C* **2015**, *119*, 6793.
[11] S. Erbas-Cakmak, S. Kolemen, A. C. Sedgwick, T. Gunnlaugsson, T. D. James, J. Yoon, E. U. Akkaya, *Chem. Soc. Rev.* **2018**, *47*, 2228.
[12] O. A. Bozdemir, R. Guliyev, O. Buyukcakir, S. Selcuk, S. Kolemen, G. Gulseren, T. Nalbantoglu, H. Boyaci, E. U. Akkaya, *J. Am. Chem. Soc.* **2010**, *132*, 8029.
[13] L. M. Adleman, *Science* **1994**, *266*, 1021.
[14] A. P. de Silva, N. D. McClenaghan, *Chem. Eur. J.* **2004**, *10*, 574.
[15] T. H. Lee, J. I. Gonzalez, J. Zheng, R. M. Dickson, *Acc. Chem. Res.* **2005**, *38*, 534.
[16] A. P. de Silva, S. Uchiyama, *Nat. Nanotechnol.* **2007**, *2*, 399.
[17] U. Pischel, *Angew. Chem., Int. Ed.* **2007**, *46*, 4026.
[18] S. C. Burdette, *Eur. J. Inorg. Chem.* **2015**, *2015*, 5728.
[19] J. F. Callan, A. P. de Silva, J. Ferguson, A. J. M. Huxley, A. M. O'Brien, *Tetrahedron* **2004**, *60*, 11125.
[20] D. P. Kennedy, C. D. Incarvito, S. C. Burdette, *Inorg. Chem.* **2010**, *49*, 916.
[21] D. Tzeli, I. D. Petsalakis, G. Theodorakopoulos, *Phys. Chem. Chem. Phys.* **2016**, *18*, 32132.
[22] D. C. Magri, G. J. Brown, G. D. McClean, A. Prasanna de Silva, *J. Am. Chem. Soc.* **2006**, *128*, 4950.
[23] D. C. Magri, M. C. Fava, C. J. Mallia, *Chem. Commun.* **2014**, *50*, 1009.
[24] G. Naren, S. Li, J. Andréasson, *Chem. Phys. Chem.* **2017**, *18*, 1726.
[25] E. U. Akkaya, E. Katz, U. Pischel, *Chem. Phys. Chem.* **2017**, *18*, 1665.
[26] G. J. Scerri, M. Cini, J. S. Schembri, P. F. da Costa, A. D. Johnson, D. C. Magri, *Chem. Phys. Chem.* **2017**, *18*, 1742.
[27] M. Baroncini, M. Semeraro, A. Credi, *Chem. Phys. Chem.* **2017**, *18*, 1755.
[28] M. L. Wood, S. Domanskyi, V. Privman, *Chem. Phys. Chem.* **2017**, *18*, 1773.
[29] B. O. F. McKinney, B. Daly, C. Yao, M. Schroeder, A. P. de Silva, *Chem. Phys. Chem.* **2017**, *18*, 1760.
[30] B. Fresch, F. Remacle, R. D. Levine, *Chem. Phys. Chem.* **2017**, *18*, 1782.
[31] M. Gamella, M. Privman, S. Bakshi, A. Melman, E. Katz, *Chem. Phys. Chem.* **2017**, *18*, 1811.
[32] A. Adamatzky, *Chem. Phys. Chem.* **2017**, *18*, 1822.
[33] S. Sreejith, A. Ajayaghosh, *India J. Chem.* **2012**, *51A*, 47.
[34] M. Massey, I. L. Medintz, M. G. Ancona, W. R. Algar, *ACS Sens.* **2017**, *2*, 1205.
[35] D. Tzeli, I. D. Petsalakis, G. Theodorakopoulos, *Int. J. Quantum Chem.* **2019**, *119*, e25958.
[36] A. P. de Silva, N. D. McClenaghan, *J. Am. Chem. Soc.* **2000**, *122*, 3965.
[37] H. T. Baytekin, E. U. Akkaya, *Org. Lett.* **2000**, *2*, 1725.
[38] B. Valeur, I. Leray, *Inorg. Chem. Acta* **2007**, *360*, 765.
[39] S. M. S. Núñez, E. Oliveira, H. M. Santos, J. L. Capelo, C. Lodeiro, *Chem. Open* **2014**, *3*, 190.
[40] A. R. Chowdhury, P. Ghosh, B. G. Roy, S. K. Mukhopadhyay, P. Mitrae, P. Banerjee, *RSC Adv.* **2015**, *5*, 62017.
[41] Z.-H. Pan, G.-G. Luo, J.-W. Zhou, J.-X. Xia, K. Fang, R.-B. Wu, *Dalton Trans.* **2014**, *43*, 8499.
[42] F. Yan, T. Zheng, S. Guo, D. Shi, Z. Han, S. Zhou, L. Chen, *Spectrochim. Acta A* **2015**, *151*, 881.
[43] Z.-D. Sun, J.-S. Zhao, X.-H. Ju, Q.-Y. Xia, *Molecules* **2019**, *24*, 3134.
[44] P. A. Panchenko, Y. V. Fedorov, O. A. Fedorova, G. Jonusauskas, *Dyes Pigm.* **2013**, *98*, 347.
[45] S. Sasaki, G. P. C. Drummen, G. Konishi, *J. Mater. Chem. C* **2016**, *4*, 2731.
[46] (a) J. P. Perdew, K. Burke, M. Ernzerhof, *Phys. Rev. Lett.* **1996**, *77*, 3865. (b) M. Enzerhof, G. E. Scuseria, *J. Chem. Phys.* **1999**, *110*, 5029. (c) C. Adamo, V. Barone, *J. Chem. Phys.* **1999**, *110*, 6158.
[47] L. A. Curtiss, M. P. McGrath, J.-P. Blaudeau, N. E. Davis, R. C. Binning Jr., L. Radom, *J. Chem. Phys.* **1995**, *103*, 6104.
[48] (a) P. J. Hay, W. R. Wadt, *J. Chem. Phys.* **1985**, *82*, 299. (b) L. E. Roy, P. J. Hay, R. L. Martin, *J. Chem. Theory Comput.* **2008**, *4*, 1029.
[49] D. Tzeli, I. D. Petsalakis, G. Theodorakopoulos, *Phys. Chem. Chem. Phys.* **2011**, *13*, 954.
[50] M. Cozi, G. Scalmani, N. Rega, V. Barone, *J. Chem. Phys.* **2002**, *117*, 43.
[51] C. P. Kelly, C. J. Cramer, D. G. Truhlar, *J. Phys. Chem. A* **2006**, *110*, 2493.
[52] D. Tzeli, P. G. Tsoungas, I. D. Petsalakis, P. Kozielewicz, M. Zloh, *Tetrahedron* **2015**, *71*, 359.
[53] H. Daver, A. G. Algarra, J. Rebek Jr., J. N. Harvey, F. Himo, *J. Am. Chem. Soc.* **2018**, *140*, 12527.
[54] (a) J. Tomasi, B. Mennucci, R. Cammi, *Chem. Rev.* **2005**, *105*, 2999. (b) A. Pedone, J. Bloino, S. Monti, G. Prampolini, V. Barone, *Phys. Chem. Chem. Phys.* **2010**, *12*, 1000.
[55] (a) M. Caricato, B. Mennucci, J. Tomasi, F. Ingrosso, R. Cammi, S. Corni, G. Scalmani, *J. Chem. Phys.* **2006**, *124*, 124520. (b) C. A. Guido, S. Caprasecca, *How to Perform Corrected Linear Response Calculations in G09*, Dipartimento di Chimica e Chimica Industriale, Università di Pisa, Pisa, **2016**.
[56] (a) D. Becke, *J. Chem. Phys.* **1993**, *98*, 1372. (b) C. Lee, W. Yang, R. G. Parr, *Phys. Rev. B* **1988**, *37*, 785.

[57] Gaussian 16, Revision B.01, M. J. Frisch, G. W. Trucks, H. B. Schlegel, G. E. Scuseria, M. A. Robb, J. R. Cheeseman, G. Scalmani, V. Barone, G. A. Petersson, H. Nakatsuji, X. Li, M. Caricato, A. V. Marenich, J. Bloino, B. G. Janesko, R. Gomperts, B. Mennucci, H. P. Hratchian, J. V. Ortiz, A. F. Izmaylov, J. L. Sonnenberg, D. Williams-Young, F. Ding, F. Lipparini, F. Egidi, J. Goings, B. Peng, A. Petrone, T. Henderson, D. Ranasinghe, V. G. Zakrzewski, J. Gao, N. Rega, G. Zheng, W. Liang, M. Hada, M. Ehara, K. Toyota, R. Fukuda, J. Hasegawa, M. Ishida, T. Nakajima, Y. Honda, O. Kitao, H. Nakai, T. Vreven, K. Throssell, J. A. Montgomery, Jr., J. E. Peralta, F. Ogliaro, M. J. Bearpark, J. J. Heyd, E. N. Brothers, K. N. Kudin, V. N. Staroverov, T. A. Keith, R. Kobayashi, J. Normand, K. Raghavachari, A. P. Rendell, J. C. Burant, S. S. Iyengar, J. Tomasi, M. Cossi, J. M. Millam, M. Klene, C. Adamo, R. Cammi, J. W. Ochterski, R. L. Martin, K. Morokuma, O. Farkas, J. B. Foresman, D. J. Fox, Gaussian, Inc., Wallingford CT, **2016**.
[58] D. Tzeli, T. Mercouris, G. Theodorakopoulos, I. D. Petsalakis, *Comput. Theoret. Chem.* **2017**, *1115*, 197.
[59] S. Kümmel, *Adv. Energy Mater.* **2017**, *7*, 1700440.
[60] I. D. Petsalakis, I. S. K. Kerkines, N. N. Lathiotakis, G. Theodorakopoulos, *Chem. Phys. Lett.* **2009**, *479*, 278.
[61] I. D. Petsalakis, G. Theodorakopoulos, O. Buchman, R. Baer, *Chem. Phys. Lett.* **2015**, *625*, 98.
[62] R. Improta, C. Ferrante, R. Bozio, V. Barone, *Phys. Chem. Chem. Phys.* **2009**, *11*, 4664.
[63] D. Tzeli, I. D. Petsalakis, G. Theodorakopoulos, *J. Phys. Chem. A* **2011**, *115*, 11749.

SUPPORTING INFORMATION

Additional supporting information may be found online in the Supporting Information section at the end of this article.

How to cite this article: Tzeli D, Petsalakis ID, Theodorakopoulos G. The solvent effect on a styryl-bodipy derivative functioning as an AND molecular logic gate. *Int J Quantum Chem.* 2020;e26181. https://doi.org/10.1002/qua.26181